Symmetry-based analytical solutions to the $\chi^{(2)}$ nonlinear directional coupler

David Barral,[1,*] Kamel Bencheikh,[1] Peter J. Olver,[2] Nadia Belabas,[1] and Juan Ariel Levenson[1]
[1]*Centre de Nanosciences et de Nanotechnologies C2N, CNRS, Université Paris-Saclay, 10 Boulevard Thomas Gobert, 91120 Palaiseau, France*
[2]*School of Mathematics, University of Minnesota, Minneapolis, Minnesota 55455, USA*

(Received 5 February 2019; published 19 April 2019)

In general, the ubiquitous $\chi^{(2)}$ nonlinear directional coupler, where nonlinearity and evanescent coupling are intertwined, is nonintegrable. We rigorously demonstrate that matching excitation to the even or odd fundamental supermodes yields dynamical analytical solutions for any phase matching in a symmetric coupler. We analyze second harmonic generation and optical parametric amplification regimes and study the influence of fundamental field parity and power on the operation of the device. These fundamental solutions are useful to develop applications in classical and quantum fields such as all-optical modulation of light and quantum-states engineering.

DOI: 10.1103/PhysRevE.99.042211

The nonlinear directional coupler (NDC) is a core device in integrated optics. Its potential was first demonstrated in $\chi^{(3)}$ materials as an all-optical switch [1,2]. The possibilities of the NDC in semiconductors were thoroughly analyzed [3]. For instance, ultrafast all-optical switching was demonstrated even though it is limited by three-photon absorption [4]. This and other interesting functionalities were later displayed in the $\chi^{(2)}$ NDC through cascaded second-order effects [5–9]. In the last years the $\chi^{(2)}$ NDC has found a flourishing field of application: quantum optics [10]. Its key strengths in quantum information processing as a source of entangled photons and entangled field quadratures have been demonstrated and are still actively explored [11–16]. In general, the $\chi^{(2)}$ NDC is a nonintegrable system and only stationary solutions—solitons—are available [17–19]. Even in this case, general solutions are only obtained numerically or in a semianalytical form [20]. The dynamical solutions of the $\chi^{(2)}$ NDC have, nonetheless, a broad range of applications in the classical and quantum regimes [5–8,10–16]. Only two limiting cases have up to now been identified as integrables, i.e., with analytical dynamical solutions: (i) The propagation equations can be reduced to those related to the simpler $\chi^{(3)}$ NDC when the phase mismatch between the fundamental and second harmonic waves propagating in the device is large, which corresponds to a regime of lower efficiency [18]. (ii) The undepleted harmonic-field approximation in spontaneous parametric downconversion linearizes the propagation equations [10].

Analytical solutions are universally preferred, since they can be used to contemplate new applications and engineer the propagation of both classical and quantum light in these devices. In this paper, we rigorously retrieve analytical solutions for the $\chi^{(2)}$ NDC for any phase matching under specific symmetry conditions: pumping in the even or odd fundamental supermode. We show, indeed, that the propagation equations are analogous to those related to a single $\chi^{(2)}$ nonlinear waveguide with imperfect phase matching. We show that in the NDC case the effective coupling plays the role of the wave-vector phase mismatch in the emblematic single waveguide [22]. We can thus analyze second harmonic generation (SHG) and optical parametric amplification (OPA) in this configuration, shedding light on the influence of total power and fundamental-modes phases on the operation of the device, towards higher efficiency and quantum applications.

The $\chi^{(2)}$ NDC, sketched in Fig. 1 (dashed box), is made of two identical nonlinear $\chi^{(2)}$ waveguides. In each waveguide, an input fundamental field at frequency ω_f is up-converted into a second harmonic field at frequency ω_h (SHG), or a weak input fundamental field is amplified with the help of a strong second harmonic field (degenerate OPA). For the sake of simplicity, we consider all fields in the same polarization mode. In the coupling region, the energy of the fundamental modes propagating in each waveguide is exchanged between the coupled waveguides through evanescent waves, whereas the interplay of the generated, or injected, second harmonic waves is negligible for the considered propagation lengths due to their high confinement into the waveguides. Both physical processes, evanescent coupling and nonlinear generation, are described by the following system of equations [5]:

$$\frac{dA_f}{dz} = iCB_f + 2igA_hA_f^* e^{i\Delta\beta z}, \quad \frac{dA_h}{dz} = igA_f^2 e^{-i\Delta\beta z},$$
$$\frac{dB_f}{dz} = iCA_f + 2igB_hB_f^* e^{i\Delta\beta z}, \quad \frac{dB_h}{dz} = igB_f^2 e^{-i\Delta\beta z}, \quad (1)$$

where A and B are the slowly varying amplitudes of fundamental (*f*) and second harmonic (*h*) fields corresponding to the upper (a) and lower (b) waveguides, respectively, g is the nonlinear constant proportional to $\chi^{(2)}$ and the spatial overlap of the fundamental and harmonic fields in each waveguide, C the linear coupling constant, $\Delta\beta \equiv \beta(\omega_h) - 2\beta(\omega_f)$ the wave-vector phase mismatch with $\beta(\omega)$ the propagation

*Corresponding author: david.barral@c2n.upsaclay.fr

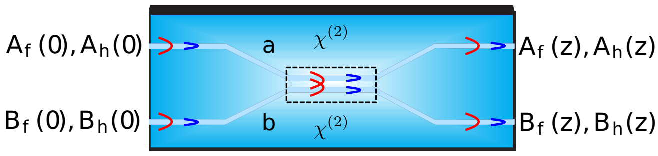

FIG. 1. Sketch of the nonlinear directional coupler $\chi^{(2)}$-NDC made of two identical waveguides a and b with second-order susceptibilities $\chi^{(2)}$. The dashed box indicates the nonlinear and coupling region. Input fundamental fields produce second harmonic fields through SHG, or input harmonic fields amplify injected fundamental seeds through OPA. In red, the fundamental waves, evanescently coupled (f). In blue, and more confined, the noninteracting second harmonic waves (h).

constant at frequency ω, and z is the coordinate along the direction of propagation. C and g are taken as real without loss of generality. We consider $C = 8 \times 10^{-2}$ mm^{-1}, $g = 25 \times 10^{-4}$ mm^{-1} mW$^{-1/2}$, and lengths of few centimeters in the simulations we show below. These are state-of-the-art values in periodically poled lithium niobate waveguides [23]. The input powers used in the simulations are of the order of those in [8].

In order to solve the set of Eqs. (1), we use dimensionless amplitudes and phases related to the complex amplitudes through

$$u_f(z) = \frac{|A_f(z)|}{\sqrt{P}}, \quad v_f(z) = \frac{|B_f(z)|}{\sqrt{P}},$$
$$\theta_f(z) = \arg\{A_f(z)\}, \quad \phi_f(z) = \arg\{B_f(z)\},$$
$$u_h(z) = \sqrt{\frac{2}{P}}|A_h(z)|, \quad v_h(z) = \sqrt{\frac{2}{P}}|B_h(z)|,$$
$$\theta_h(z) = \arg\{A_h(z)\}, \quad \phi_h(z) = \arg\{B_h(z)\},$$

with $P = |A_f|^2 + |B_f|^2 + 2|A_h|^2 + 2|B_h|^2$ the total input power. We also introduce a normalized propagation coordinate $\zeta \equiv \sqrt{2P}gz$, which is defined only in the nonlinear and coupling region (Fig. 1, dashed box). Applying this change of variables into Eq. (1), we obtain for the modes propagating in waveguide a,

$$\frac{du_f}{d\zeta} = -\kappa\, v_f \sin(\delta_f) - u_f u_h \sin(\Delta\theta), \tag{2}$$
$$\frac{d\theta_f}{d\zeta} = \kappa \frac{v_f}{u_f}\cos(\delta_f) + u_h\cos(\Delta\theta), \tag{3}$$
$$\frac{du_h}{d\zeta} = u_f^2 \sin(\Delta\theta), \tag{4}$$
$$\frac{d\theta_h}{d\zeta} = \frac{u_f^2}{u_h}\cos(\Delta\theta), \tag{5}$$

and for the modes propagating in waveguide b,

$$\frac{dv_f}{d\zeta} = \kappa\, u_f \sin(\delta_f) - v_f v_h \sin(\Delta\phi), \tag{6}$$
$$\frac{d\phi_f}{d\zeta} = \kappa \frac{u_f}{v_f}\cos(\delta_f) + v_h\cos(\Delta\phi), \tag{7}$$
$$\frac{dv_h}{d\zeta} = v_f^2 \sin(\Delta\phi), \tag{8}$$
$$\frac{d\phi_h}{d\zeta} = \frac{v_f^2}{v_h}\cos(\Delta\phi). \tag{9}$$

The three governing parameters of the system are the effective coupling $\kappa \equiv C/(\sqrt{2P}g)$, the fundamental field phase difference $\delta_f \equiv \phi_f - \theta_f$, and the nonlinear phase mismatches $\Delta\theta \equiv \theta_h - 2\theta_f + \Delta S\zeta$ and $\Delta\phi \equiv \phi_h - 2\phi_f + \Delta S\zeta$, where $\Delta S = \Delta\beta/(\sqrt{2P}g)$ is an effective wave-vector phase mismatch. Remarkably, the nonlinear phase mismatch drives the nonlinear optical processes, whereas the effective coupling indicates which effect is stronger, either the evanescent coupling or the nonlinear interaction. Additionally, there are two dynamical invariants, the energy and momentum of the total system, given respectively by

$$u_f^2 + v_f^2 + u_h^2 + v_h^2 = 1, \tag{10}$$

$$u_h u_f^2 \cos(\Delta\theta) + v_h v_f^2 \cos(\Delta\phi) + 2\kappa u_f v_f \cos(\delta_f) = \Gamma, \tag{11}$$

where Γ is a constant given by the initial conditions [24].

The systems of Eqs. (2)–(5) and (6)–(9) are not integrable in general [18]. The key to our analytical solution is to take advantage of the fact that the full system of Eqs. (2)–(9) is invariant under the following set of transformations $F(u_f, \theta_f, u_h, \theta_h, v_f, \phi_f, v_h, \phi_h)$:

$$u_f \leftrightarrow v_f, \quad u_h \leftrightarrow v_h,$$
$$\phi_f \leftrightarrow \theta_f + n\pi, \quad \Delta\theta \leftrightarrow \Delta\phi, \tag{12}$$

with $n = 0, 1$. The two last transformations can be combined to obtain $\phi_h \leftrightarrow \theta_h$. In general, this set of transformations modifies the initial conditions of the problem, thus losing the symmetry and the dynamical invariance. Nonetheless, we crucially notice that for symmetric initial conditions,

$$u_f(0) = v_f(0), \quad u_h(0) = v_h(0),$$
$$\phi_f(0) = \theta_f(0) + n\pi, \quad \phi_h(0) = \theta_h(0), \tag{13}$$

the symmetry relations between the field amplitudes and phases persist along propagation, protected by the invariance of Eqs. (2)–(9), so that at all z,

$$u_f = v_f, \quad u_h = v_h,$$
$$\phi_f = \theta_f + n\pi, \quad \phi_h = \theta_h. \tag{14}$$

These relations were mentioned along the analysis of the stationary solutions to Eqs. (1) [18]. However, the connection between the initial conditions Eqs. (13) and the solution Eqs. (14) was missing. We proceed here to give rigorous justification to Eqs. (14). Let us rewrite Eqs. (2)–(5) and (6)–(9) as a single vector equation,

$$\frac{d\mathbf{x}}{d\zeta} = h(\mathbf{x}), \tag{15}$$

with $\mathbf{x} = (u_f, \theta_f, u_h, \theta_h, v_f, \phi_f, v_h, \phi_h)^T$. Let F be the locally defined invertible differentiable map which is given by Eqs. (12). Then, by the chain rule, $\mathbf{y}(\zeta) = F(\mathbf{x}(\zeta))$ solves the system of ordinary differential equations

$$dy/d\zeta = H(\mathbf{y}) = \nabla F(F^{-1}(\mathbf{y}))h(F^{-1}(\mathbf{y})),$$

where $\nabla F(\mathbf{x})$ denotes the Jacobian matrix of F at $\mathbf{x}$. Now suppose $H = h$ on their common domain of definition, meaning that the map F defines a symmetry of Eq. (15). Furthermore, suppose F is also a symmetry of the initial conditions $\mathbf{x}(0) = \mathbf{x}_0$ such that $F(\mathbf{x}_0) = \mathbf{x}_0$. Then $\mathbf{x}(\zeta)$ and $\mathbf{y}(\zeta)$ both solve the same initial value problem. Hence, since the system is smooth (indeed analytic), by uniqueness of solutions to the initial value problem, they must be the same, meaning that F is also a symmetry of the solution:

$$\mathbf{x}(\zeta) = F(\mathbf{x}(\zeta)), \tag{16}$$

which proves Eqs. (14). This proof is, indeed, general; any system with smooth evolution and invariant under an invertible and differentiable transformation F has solutions that retain this invariance provided the initial conditions are also F invariant. This result is related to century-old questions concerning the impact of symmetries on physical systems, formulated by Curie and Lie [21].

The symmetry of the solutions Eq. (16) thus simplifies the system of Eqs. (2)–(9) into

$$\frac{du_f}{d\zeta} = -u_f u_h \sin(\Delta\theta), \tag{17}$$

$$\frac{du_h}{d\zeta} = u_f^2 \sin(\Delta\theta), \tag{18}$$

$$\frac{d\Delta\theta}{d\zeta} = \left(\frac{u_f^2}{u_h} - 2u_h\right)\cos(\Delta\theta) - (-1)^n 2\kappa, \tag{19}$$

and the dynamical invariants Eqs. (10) and (11) into

$$u_f^2 + u_h^2 = 1/2, \qquad v_f^2 + v_h^2 = 1/2, \tag{20}$$

$$\left(1 - 2u_h^2\right)(u_h \cos(\Delta\theta) + (-1)^n\kappa) = \Gamma. \tag{21}$$

Remarkably, these equations are analogous to those related to the nonlinear interaction of two waves with imperfect phase matching $\Delta\beta$ in a bulk crystal or single waveguide [22]. In our case, the effective coupling 2κ plays the role of $\Delta\beta$ in the crystal or single waveguide. The reduced equations (17)–(19) are fulfilled only when harmonic and fundamental input powers are set equal in each waveguide, $u_f^2(0) = v_f^2(0)$ and $u_h^2(0) = v_h^2(0)$, harmonic fields in phase, $\theta_h(0) = \phi_h(0)$, and fundamental fields either in phase, $\theta_f(0) = \phi_f(0)$, or π-dephased, $\theta_f(0) = \phi_f(0) + \pi$. This leads to a reasonable set of initial conditions for the $\chi^{(2)}$ NDC, as these conditions correspond to the excitation of the even or odd fundamental eigenmodes of the linear directional coupler, so-called supermodes [25]. Outstandingly, the $\chi^{(2)}$ NDC is a versatile source of quantum entanglement under these conditions [14–16].

Equations (17)–(19) have analytical solutions in terms of Jacobi elliptic functions [22]. We analyze thoroughly these solutions in the SHG and OPA regimes. From Eqs. (18) and (21) we get

$$\zeta = \pm\frac{1}{2}\int_{u_h^2(0)}^{u_h^2(\zeta)} \frac{d\left(u_h^2\right)}{\sqrt{u_h^2\left(\frac{1}{2} - u_h^2\right)^2 - \left[\frac{\Gamma}{2} - (-1)^n\kappa\left(\frac{1}{2} - u_h^2\right)\right]^2}}. \tag{22}$$

The expression in the square root has three roots, $u_{h,3}^2 > u_{h,2}^2 > u_{h,1}^2 \geqslant 0$. By using the function y and the parameter γ, defined respectively as $y^2 = (u_h^2 - u_{h,1}^2)/(u_{h,2}^2 - u_{h,1}^2)$ and $\gamma^2 = (u_{h,2}^2 - u_{h,1}^2)/(u_{h,3}^2 - u_{h,1}^2)$, we can rewrite Eq. (22) as

$$\zeta = \frac{\pm 1}{2\sqrt{u_{h,3}^2 - u_{h,1}^2}}\int_{y(0)}^{y(\zeta)} \frac{dy}{\sqrt{(1-y^2)(1-\gamma^2 y^2)}}.$$

y is the Jacobi elliptic function of ζ. The normalized harmonic power is thus given by

$$u_h^2 = u_{h,1}^2 + \left(u_{h,2}^2 - u_{h,1}^2\right)\,\mathrm{sn}^2\left[\sqrt{u_{h,3}^2 - u_{h,1}^2}(\zeta + \zeta_0), \gamma\right], \tag{23}$$

where sn stands for the Jacobi elliptic sine. ζ_0 is determined by the initial condition $u_h^2(0)$ and the parameter γ, and it is given by

$$\zeta_0 = \frac{1}{\sqrt{u_{h,3}^2 - u_{h,1}^2}}\,\mathrm{arcsn}\left[\sqrt{\frac{u_h^2(0) - u_{h,1}^2}{u_{h,2}^2 - u_{h,1}^2}}, \gamma\right],$$

where arcsn stands for the inverse Jacobi elliptic sine. The period of oscillations in the harmonic powers is thus

$$L = \frac{2K(\gamma)}{\sqrt{u_{h,3}^2 - u_{h,1}^2}}, \tag{24}$$

with K the complete elliptic integral of first kind. The individual phases $\theta_{f,h}$ and the nonlinear phase mismatch $\Delta\theta$ can be straightforwardly obtained from Eqs. (3), (5), and (23), and the invariants given by Eqs. (20) and (21).

Now we show the solutions for two specific cases of SHG and OPA. We consider perfect wave-vector phase matching $\Delta\beta = 0$ in both situations for the sake of simplicity. For SHG $u_h^2(0) = 0$ and $\Gamma = (-1)^n\kappa$, so that the roots from the expression in the square root of Eq. (22) are solutions of

$$u_h^6 - (1+\kappa^2)u_h^4 + \frac{u_h^2}{4} = 0,$$

which read

$$u_{h,1}^2 = 0, \quad u_{h,2(3)}^2 = \frac{1 + \kappa^2 \pm \kappa\sqrt{2+\kappa^2}}{2}. \tag{25}$$

Notably, these solutions depend only on the strength of the effective coupling κ and not on the supermode parity, i.e., not on n. This point is clarified in the analysis of the nonlinear phase mismatch evolution below.

Figure 2 displays the dimensionless powers [Eqs. (23) and (25)] for each mode in waveguide a (or equally b) along the propagation in the SHG regime. We have set $\kappa = 0.51$, equivalent to $P = 2\,W$ for our realistic values, in lithium niobate. A strong fundamental field depletion and a periodic switch from fundamental-to-harmonic conversion to harmonic-to-fundamental conversion are observed. $L = 3.35$ is the period of oscillation analytically calculated through Eq. (24). $L/2$

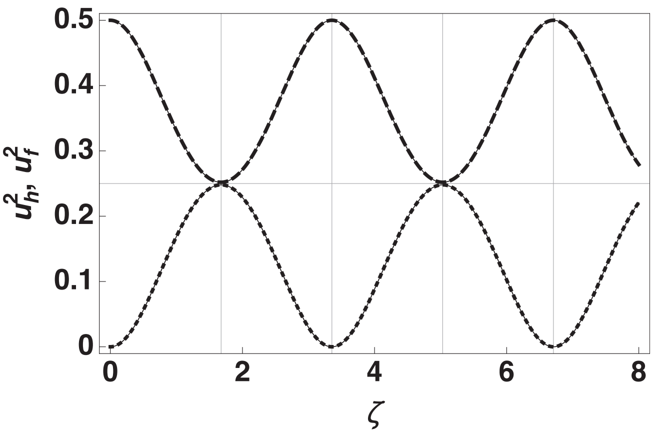

FIG. 2. Fundamental (upper curve) and harmonic (lower curve) field power propagation in the SHG regime. Dimensionless fundamental power u_f^2 (dash) and second harmonic power u_h^2 (dot). $\kappa = 0.51$. The vertical lines show the effective coupling coherence length $L/2$, with $L = 3.35$ the oscillation period analytically calculated. ζ is the normalized propagation coordinate. $\zeta = 1$ stands for $z \equiv (\sqrt{2P}g)^{-1} = 6.3$ mm.

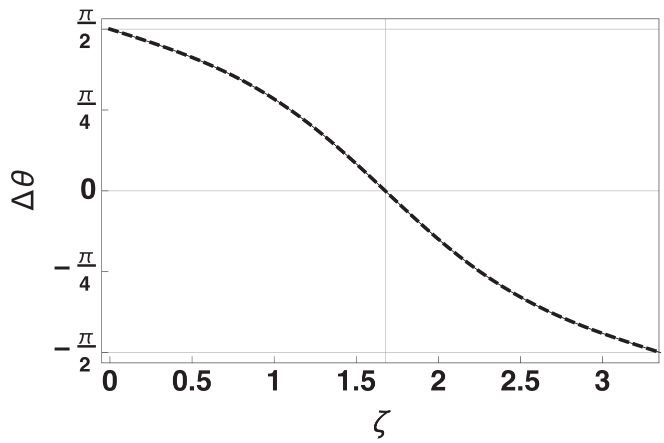

FIG. 3. Nonlinear phase mismatch evolution along propagation in one oscillation period L in the SHG regime (dash). $\kappa = 0.51$ and $n = 0$. The vertical line shows the effective coupling coherence length $L/2$, with $L = 3.35$ the oscillation period analytically calculated. ζ is the normalized propagation coordinate. $\zeta = 1$ stands for $z \equiv (\sqrt{2P}g)^{-1} = 6.3$ mm.

is the effective coupling coherence length defined in analogy with the wave-vector coherence length. The connection of the observed periodic behavior and a coupling-based nonlinear phase mismatch has been proposed recently through the analysis of numerical simulations [15,16]. To clarify the origin of these periodic oscillations, we calculate the evolution of phases along propagation. The individual phases are given by

$$\theta_h(\zeta) = \theta_h(0) + (-1)^n\kappa\,\zeta,$$
$$\theta_f(\zeta) = \theta_f(0) + \frac{(-1)^n\kappa}{u_{h,3}}\,\Pi[2u_{h,2}^2, \Phi(u_{h,3}\zeta, \gamma), \gamma], \qquad (26)$$

where Π is the elliptic integral of the third kind and Φ the amplitude of Jacobi elliptic functions. Figure 3 shows the evolution of the nonlinear phase mismatch $\Delta\theta(\zeta)$ in a period of oscillation L. We set κ as above, $\theta_f(0) = 0$ and $\theta_h(0) = \pi/2$, due to the well-known SHG phase jump [22]. The phase mismatch evolves from $\pi/2$ down to $-\pi/2$ in an oscillation period L when the parity is set as $n = 0$ (Fig. 3). A symmetric evolution curve from $\pi/2$ up to $3\pi/2$ is obtained for $n = 1$ (not shown). Since the evolution of $\sin(\Delta\theta)$, and thus of the u_f and u_h solutions in Eqs. (17) and (18), is the same in both cases, SHG is independent of the input supermode parity. Equations (26) show that the linear coupling of the fundamental modes κ produces a nonlinear phase mismatch which cyclically destroys the wave-vector phase matching initially fulfilled, driving two successive nonlinear optical processes, upconversion in the first effective coupling coherence length followed by downconversion in the second coupling length. We stress that our analytical solutions perfectly match with the numerical solutions of Eqs. (2)–(9).

For OPA with a set of input phases such that $\Delta\theta(0) = 0$, $\Gamma = u_h(0) - 2u_h^3(0) + (-1)^n\kappa\,(1 - 2u_h^2(0))$ is preserved along propagation, and the roots of the expression in the square root of Eq. (22) are given by solving the expression

$$u_h^2\left(\frac{1}{2} - u_h^2\right)^2 - \left[\frac{u_h(0)}{2} - u_h^3(0) + (-1)^n\kappa\,\left(u_h^2 - u_h^2(0)\right)\right]^2 = 0,$$

with general solutions

$$u_{h,1}^2 = u_h^2(0), \quad u_{h,2(3)}^2 = \frac{1}{2}\left[1 - u_h^2(0) + \kappa^2 \mp \sqrt{2u_h^2(0)\left(1 - 3\kappa^2 - \frac{3}{2}u_h^2(0)\right) + 4(-1)^n\kappa\, u_h^2(0)\big(1 - 2u_h^2(0)\big) + \kappa^2(2 + \kappa^2)}\right]. \qquad (27)$$

These solutions also include SHG when $u_h^2(0) = 0$. Note that Eqs. (27) have to be suitably ordered in order to be used in Eq. (23). In contrast to SHG, Eqs. (27) depend in this case on the input harmonic power $u_h^2(0)$, the effective coupling κ, and the parity of the input fundamental supermode via the parameter n. We show below the dependence of the solutions on parity and input harmonic power.

Figure 4(a) displays the dimensionless fundamental powers [Eqs. (23) and (27)] in waveguide a (or equally b) along the propagation in a specific case of OPA. We have set $u_h^2(0) = 0.499$, $\kappa = 0.92$ ($P = 600$ mW), and $n = 0$ [Fig. 4(a), black dash] and $n = 1$ [Fig. 4(a), gray dash]. The harmonic fields are not shown, since they remain almost undepleted for this set of parameters. Note that the power scale (ordinate axis) has been expanded by a factor of 10^3. In contrast with SHG, OPA depends on the parity of the input fundamental supermodes. The system periodically switches from harmonic-to-fundamental conversion to

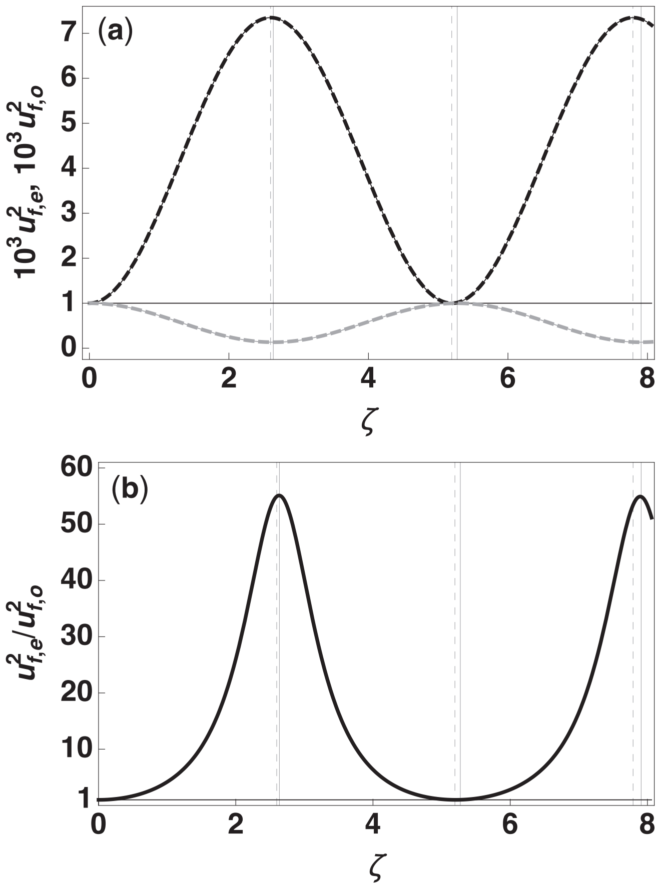

FIG. 4. (a) Fundamental field power propagation in the OPA regime for an even and odd input fundamental supermode. Even dimensionless fundamental power $u_{f,e}^2$ (dash, black). Odd dimensionless fundamental power $u_{f,o}^2$ (dash, gray). (b) Ratio between even and odd fundamental field power $u_{f,e}^2/u_{f,o}^2$ (solid, black) along propagation. $\kappa = 0.92$. The vertical lines show the even and odd effective coupling coherence lengths $L_{\text{even}}/2$ (dash) and $L_{\text{odd}}/2$ (solid), with $L_{\text{even}} = 5.19$ and $L_{\text{odd}} = 5.27$ analytically calculated. ζ is the normalized propagation coordinate. $\zeta = 1$ stands for $z \equiv (\sqrt{2P}g)^{-1} = 11.5$ mm.

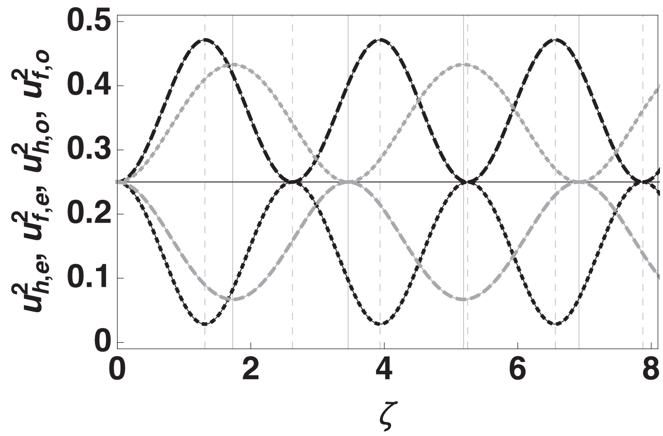

FIG. 5. Fundamental (dash) and harmonic (dot) field power propagation in the OPA regime for an even (black) and odd (gray) input fundamental supermode. Even dimensionless fundamental and harmonic power $u_{f(h),e}^2$ [dash (dot), black]. Odd dimensionless fundamental and harmonic power $u_{f(h),o}^2$ [dash (dot), gray]. $\kappa = 0.92$. The vertical lines show the even and odd effective coupling coherence lengths $L_{\text{even}}/2$ (dash) and $L_{\text{odd}}/2$ (solid), with $L_{\text{even}} = 2.62$ and $L_{\text{odd}} = 3.46$ analytically calculated. ζ is the normalized propagation coordinate. $\zeta = 1$ stands for $z \equiv (\sqrt{2P}g)^{-1} = 11.5$ mm.

fundamental-to-harmonic conversion for even input parity, whereas it switches from fundamental-to-harmonic conversion to harmonic-to-fundamental conversion for odd input parity. Unlike in SHG, the nonlinear phase mismatch $\Delta\theta$ evolves in OPA from the initial value $\Delta\theta(0) = 0$ to negative ($n = 0$) or positive ($n = 1$) values (not shown). This modifies the evolution of the amplitudes $u_{f,h}$ through the sign of $\sin(\Delta\theta)$ in Eqs. (17) and (18). The period of oscillation is also modified by the input parity with $L_{\text{even}} = 5.19$ and $L_{\text{odd}} = 5.27$. At $L_{\text{odd}}/2$ the fundamental odd mode is reduced by approximately a factor of 7.5, whereas at $L_{\text{even}}/2$ the fundamental even mode is amplified by the same factor. Figure 4(b) displays the ratio between even and odd fundamental field powers $u_{f,e}^2/u_{f,o}^2$ along propagation. Notably, a ratio higher than 50 is obtained at the odd effective coupling coherence length $L_{\text{odd}}/2$.

Figure 5 displays the dimensionless fundamental and harmonic powers [Eqs. (23) and (27)] in waveguide *a* (or equally *b*) along propagation in the OPA regime for equal injection of fundamental and harmonic fields, i.e., $u_h^2(0) = 0.25$. For the sake of comparison, the effective coupling is set as above ($\kappa = 0.92$). We show the evolution of the fields produced by injection of even (black) or odd (gray) fundamental supermodes at the input. Fundamental and harmonic fields are in dash and dot, respectively. Strong harmonic field depletion and fundamental field amplification are achieved for even ($n = 0$) input. Lower fundamental field depletion and harmonic field amplification are obtained for odd ($n = 1$) input. Shorter periods of oscillation and larger even-odd oscillation period shifts are observed in comparison with those in Fig. 4. The even configuration allows switching from harmonic undepletion to a large amount of depletion at $L_{\text{even}}/2$ by either injection of no, or very small, fundamental seed, as in Fig. 4, or a substantial fundamental seed, as in Fig. 5. We have also found that the higher the total input power P, the larger the harmonic field depletion (not shown). In contrast, the odd configuration yields the converse effect: the harmonic fields are amplified when substantial fundamental seeds are injected. Hence, two mechanisms, parity and power of the fundamental supermode, can be used as modulation parameters for a $\chi^{(2)}$ NDC all-optical switch. The analytical solutions enable prediction of the amplitude and period of oscillation of the optical fields along propagation through Eqs. (23) and (24), respectively. It is then possible to appropriately fix the initial conditions for the desired operating mode, even in the quantum regime [15,16].

In conclusion, we have studied the $\chi^{(2)}$ NDC and rigorously demonstrated that matching excitation to the even or odd fundamental supermodes yields dynamical analytical solutions for any phase matching. The propagation equations are analogous to those related to a single $\chi^{(2)}$ nonlinear waveguide with imperfect phase matching, but in the NDC we show that the effective coupling plays the role of the wave-vector phase mismatch. We have reviewed the SHG and OPA regimes and studied the influence of fundamental field parity and power on the operation of the device. We have investigated the possible application of this device as an all-optical switch. This study completes the analysis carried out in [15,16], where the versatility of this device as a resource for quantum information processing was shown. Finally, we want to stress that our analysis can open new avenues in the study of general coupled $\chi^{(2)}$ nonlinear systems, such as arrays of nonlinear waveguides in optics and Fermi resonance interface modes in solid-state physics [26,27]. The use of symmetries can indeed help to simplify these systems and obtain analytical solutions to understand their dynamics better [28].

ACKNOWLEDGMENTS

We thank K. Belabas for useful discussions. This work was supported by the Agence Nationale de la Recherche through the INQCA project (Grant Agreement No. PN-II-ID-JRPRO-FR-2014-0013 and ANR-14-CE26-0038), the Paris Île-de-France region in the framework of DIM SIRTEQ through the project ENCORE, and the Investissements d'Avenir program (Labex NanoSaclay, Reference ANR-10-LABX-0035).

[1] S. M. Jensen, IEEE J. Quantum Electron. **18**, 1580 (1982).
[2] A. A. Maer, Sov. J. Quantum Electron. **14**, 101 (1984).
[3] E. M. Wright, S. W. Koch, J. E. Ehrlich, C. T. Seaton, and G. I. Stegeman, Appl. Phys. Lett. **52**, 2127 (1988).
[4] A. Villeneuve, C. C. Yang, P. G. J. Wigley, G. I. Stegeman, J. S. Aitchison, and C. N. Ironside, Appl. Phys. Lett. **61**, 147 (1992).
[5] G. Assanto, G. Stegeman, M. Sheik-Bahae, and E. van Stryland, Appl. Phys. Lett. **62**, 1323 (1993).
[6] R. Schiek, Opt. Quantum. Electron. **26**, 415 (1994).
[7] R. Schiek, Y. Baek, G. Krijnen, G. I. Stegeman, I. Baumann, and W. Sohler, Opt. Lett. **21**, 940 (1996).
[8] R. Schiek, L. Fiedrich, H. Fang, G. I. Stegeman, K. R. Parameswaran, M.-H. Chou, and M. Fejer, Opt. Lett. **24**, 1617 (1999).
[9] U. Hempelmann, J. Opt. Soc. Am. B **19**, 243 (2002).
[10] J. Perina, Jr., and J. Perina, *Progress in Optics* (Elsevier, Amsterdam, 2000).
[11] R. Kruse, F. Katzschmann, A. Christ, A. Schreiber, S. Wilhelm, K. Laiho, A. Gábris, C. S. Hamilton, I. Jex, and Ch. Silberhorn, New. J. Phys. **15**, 083046 (2013).
[12] R. Kruse, L. Sansoni, S. Brauner, R. Ricken, C. S. Hamilton, I. Jex, and Ch. Silberhorn, Phys. Rev. A **92**, 053841 (2015).
[13] F. Setzpfandt, A. S. Solntsev, J. Titchener, C. W. Wu, C. Xiong, R. Schiek, T. Pertsch, D. N. Neshev, and A. A. Sukhorukov, Laser Photonics Rev. **10**, 131 (2016).
[14] J. Herec, J. Fiurasek, and L. Mista, Jr., J. Opt. B: Quantum Semiclassical Opt. **5**, 419 (2003).
[15] D. Barral, N. Belabas, L. M. Procopio, V. D'Auria, S. Tanzilli, K. Bencheikh, and J. A. Levenson, Phys. Rev. A **96**, 053822 (2017).
[16] D. Barral, K. Bencheikh, V. D'Auria, S. Tanzilli, N. Belabas, and J. A. Levenson, Phys. Rev. A **98**, 023857 (2018).
[17] W. C. K. Mak, B. A. Malomed, and P. L. Chu, Phys. Rev. E **55**, 6134 (1997).
[18] O. Bang, P. L. Christiansen, and C. B. Clausen, Phys. Rev. E **56**, 7257 (1997).
[19] W. C. K. Mak, B. A. Malomed, and P. L. Chu, Phys. Rev. E **57**, 1092 (1998).
[20] W. C. K. Mak, B. A. Malomed, and P. L. Chu, Opt. Commun. **154**, 145 (1998).
[21] J. Ismael, Synthese **110**, 167 (1997).
[22] J. A. Armstrong, N. Bloembergen, J. Ducuing, and P. S. Pershan, Phys. Rev. **127**, 1918 (1962).
[23] O. Alibart, V. D'Auria, M. De Micheli, F. Doutre, F. Kaiser, L. Labonté, T. Lunghi, E. Picholle, and S. Tanzilli, J. Opt. **18**, 104001 (2016).
[24] In terms of the original amplitudes, the momentum is given by $\Gamma = g(A_h A_f^{*2} + B_h B_f^{*2}) + CA_f B_f^* + \text{c.c.}$, where c.c. stands for complex conjugate. It is obtained from the flux of momentum of the electromagnetic stress-energy-momentum tensor. Equations (1) are derived from this momentum. For a quantum mechanical introduction, see, for instance, M. Toren and Y. Ben-Aryeh, Quantum Opt. **6**, 425 (1994).
[25] A. Yariv, *Quantum Electronics* (John Wiley & Sons, New York, 1988).
[26] F. Setzpfandt, A. A. Sukhorukov, D. N. Neshev, R. Schiek, Y. S. Kivshar, and T. Pertsch, Phys. Rev. Lett. **105**, 233905 (2010).
[27] V. M. Agranovich, *Excitations in Organic Solids* (Oxford University Press, New York, 2008).
[28] D. Barral, K. Bencheikh, N. Belabas, and J. A. Levenson, arXiv:1903.10074.